Chapter 6
Grinding Wheel Micro-design—Abrasive Layer and Wear

> *The performance of a grinding wheel, however, is not only a complicated function of all grinding wheel parameters such as grain nature and grain dimensions, nature of bond material, volumetric composition of the wheel* etc.*, but, as said before, depends on the grinding conditions also* [DECN70].

Micro-design of grinding wheels, i.e. structure and composition of the abrasive layer, follows from the tool components and manufacturing processes as described in the preceding chapters and affects tool performance significantly. The tool topography in the form of the cutting edge density results from the abrasive layer composition and will be characterized in Sect. 6.2 "Cutting Edge Density". Since grinding wheels wear constantly, tool wear effects (what?, Sect. 6.3) and mechanisms (why?, Sect. 6.4) need to be considered comprehensively when evaluating tool performance. Tool conditioning is a means to secure defined tool profile and sharpness and will also be introduced in Sect. 6.5. This knowledge will allow first discussions of sustainability about tool micro-design and wear at the end of the chapter.

Grinding tool performance is evaluated by several characteristics:

- Grinding ratio G,
- Specific grinding energy,
- Workpiece surface roughness,
- Heat flow into workpiece surface layer,
- Grinding forces in tangential and normal direction F_t and F_n,
- Grinding force ratio μ between tangential and normal grinding force, etc.

These characteristics are not only affected by the process design, but significantly by the tool design as described in the following.

B. Linke, *Life Cycle and Sustainability of Abrasive Tools*,
RWTHedition, DOI 10.1007/978-3-319-28346-3_6

6.1 Abrasive Layer Composition

6.1.1 Volumetric Composition

The percentages of grit volume, V_G, bond volume, V_B, and pore volume, V_P, add up to 100 % (Eq. 6.1). The mass, m, of the abrasive layer is composed of the grit mass and bonding mass, defined by their respective densities, ρ_G and ρ_B (Eq. 6.2).

$$V_G + V_B + V_P = 100\,\% \tag{6.1}$$

$$m = m_G + m_B = \rho_G V_G + \rho_B V_B \tag{6.2}$$

The volumetric composition of grits, bond and pores can be displayed in ternary diagrams (Fig. 6.1). The phase diagram in Fig. 6.1 displays the lines with iso-properties, such as iso-grit volume, iso-bond volume, iso-porosity, and iso-grit-bond ratio [DECN70, MALK08, p. 31 ff]. The iso-grit lines are often considered as "iso-structure lines" [DECN70]. Moreover, the iso-grit lines commonly define the packing number in conventional wheel designations or in the concentration number for superabrasive wheels [MALK08, p. 32].

Maximum packing density is obtained by shaking and pressing the grinding wheel mixture before hardening or sintering; a tool with lower packing density still needs to have enough grit contact, so that the tool does not loose its shape during hardening or sintering [DECN70].

Lines with iso-grit-bond ratio in Fig. 6.1 all pass through one tip of the ternary phase diagram, V_p, where the abrasive layer theoretically has 100 % porosity [DECN70]. The maximum grit-bond ratio with the minimum bond equivalent is defined by strength requirements of the abrasive tool body; minimum grit-bond ratio is imposed by practical manufacturing experience [DECN70].

Several researchers have displayed the most common ranges of grinding tool compositions in ternary diagrams (Fig. 6.2) [KLOC09, p. 45, MENA00, MARI07, p. 111, MALK08, p. 31]. The boundaries for these ranges can be overcome by adding artificial pore builders or using hot pressing methods [KLOC09, p. 45]. In

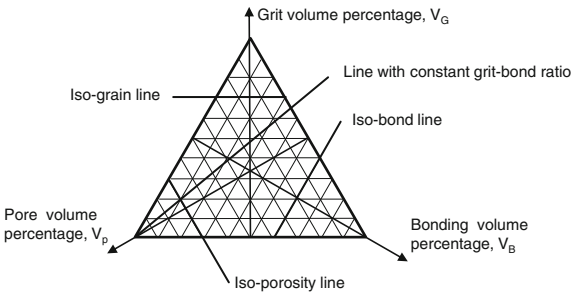

Fig. 6.1 Phase diagram of abrasive layers with iso lines [MALK08, p. 31 ff, DECN70]

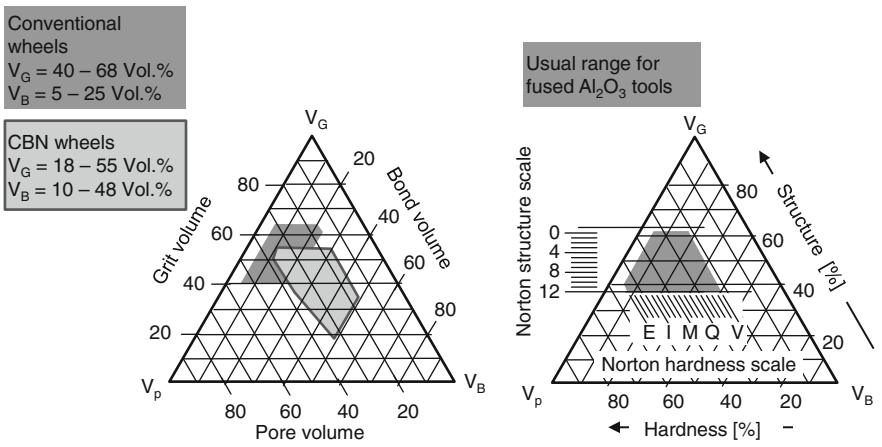

Fig. 6.2 Phase diagram of abrasive layers, *left* typical compositions of conventional and CBN wheels, after [KLOC09, p. 45]; *right* simplified mapping of hardness and structure scale to corundum wheels, after [MENA00]

general, superabrasive grinding wheels have a lower volumetric percentage of abrasive grits [METZ86, p. 52].

The simplified diagram in Fig. 6.2 right suggests that the hardness coincides with the iso-porosity lines for the shown grinding wheel brand [MENA00]. For most grinding wheels, however, hardness grade does not usually coincide with the iso-porosity lines and wheel manufacturers have more complex hardness lines in the ternary diagram [MALK08, p. 33, DECN70]. Grit concentrations for CBN tools tend to be higher than for diamond wheels (up to 50 % by volume), especially for internal and many cylindrical grinding applications [MARI04, p. 419]. Therefore, the structure number of CBN wheels is limited to a smaller range [MARI04, p. 419].

Higher bonding proportion with a constant grit proportion leads to thicker bonding bridges holding the abrasive grits tighter (Fig. 6.3 (a) and (b)). This results in increasing wheel strength, Young's modulus, hardness, and density [KLOM86].

The amounts of grit and bond content can be calculated either by keeping the bonding specification constant and varying the grit concentration or by varying both bonding specification and grit concentration. A common approach is to calculate the grit volume, V_g, from Eq. 6.3 corresponding to the structure number, N_s [BORK92, p. 35, MALK08, p. 16].

$$V_G = (62 - 2N_s)\% \tag{6.3}$$

N_s structure number in the ranges of 0–4 (close structure), 5–8 (medium), 9–14 (wide structure)

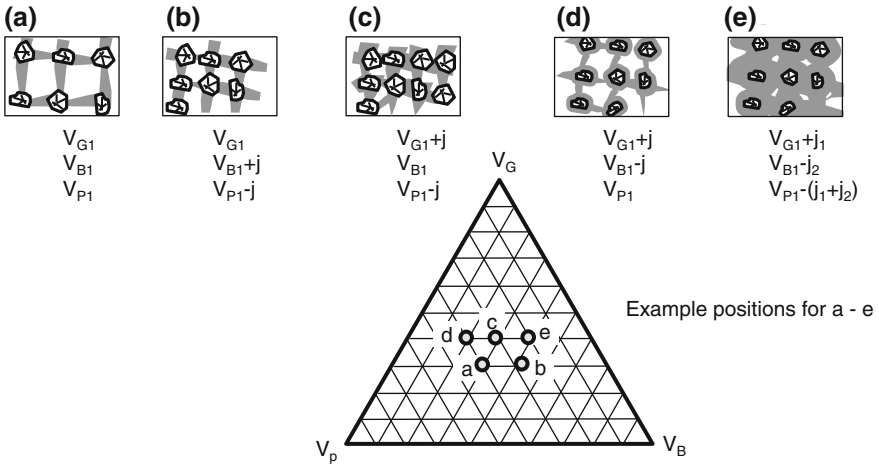

Fig. 6.3 Examples for different wheel compositions after [KLOC09]

Achieving balanced composition is a complex task (Fig. 6.3). Increased bond volume at constant grit volume leads to stronger bond bridges and raises the overall bending resistance and elasticity [BOTS05, p. 92]. A high bond volume might lead to a high proportion of grit splintering resulting from the strong retention force [BOTS05, p. 93]. A bigger grit volume implies more active cutting edges and decreases the load for the single grit resulting in less wear but increased friction.

Homogeneous distribution of abrasive grits, bonding material, and pores in the abrasive layer is crucial for a constant process performance. A non-uniform distribution of abrasive material leads to an uneven material removal process and respectively to a change in the chip thickness. This results in varying loads on the grits, affecting generated workpiece surface as well as wear behavior of the grinding wheel [KLOC05c].

Bot-Schulz published micro-computer-tomography (CT) pictures of a vitrified grinding tool sample for the first time [BOTS05, p. 108 f.]. Challenges lie within the resolution of the computer tomography microscope and the small differences between the densities of the vitrified bonding, the sol-gel corundum grits, and the white corundum grits as secondary grit material. Micro-CT pictures enable the realistic modeling of the bonding bridges between grits [BOTS05, p. 108].

6.1.2 Porosity

Pores are necessary for the transport of cooling lubricant to and chips away from the cutting point. They become more critical for high material removal rates and high-speed grinding processes to get enough cooling lubricant into the grinding

gap. Grinding wheels with discontinuous cutting faces have similar effects as highly porous wheels [BORK92, p. 36].

Porosity can be influenced by the volumetric composition of abrasives and bond material via Eq. 6.1. In principle, there are two ways to actively create porosity [YARN69], by either substances burning up during tool manufacturing, or hollow substances breaking up during the abrasive machining process.

The proportion of pores varies by grinding wheel bond type. Resin bonded wheels have nearly no porosity, whereas vitrified tools can have porosity up to 70 % of volume [MARI07, p. 113]. The pores in metallic bonded grinding wheels cannot hold the cooling lubricant as well as pores in vitrified bonded tools. The active generation of pores is explained in the manufacture of vitrified bonded tools (Sect. 3.2.2 "Manufacturing of Vitrified Bonds") and sintered metallic bonded tools (Sect. 3.3.3 "Manufacturing of Metallic Bonds by Sintering"). Super-porous grinding wheels can have pores exceeding the grit size by several times [BORK92, p. 35].

Porosity of abrasive tools affects their mechanical strength. Yarnitsky [YARN69] states that an increase in porosity by 20 % can reduce the modulus of elasticity to about 60 % of its original value. The tool becomes softer and the effective dynamic hardness is affected. Pores can be seen as a discontinuity in the abrasive tool material bringing about a stress concentration. The latter can lead to cracks and fatigue fracture as consequence. The effect of the discontinuity, however, depends on the bonding system, geometric pore structure, pore size, uniformity and distribution. In brittle (vitrified) bonds, the effect of material discontinuity is worse than in soft bonds like plastic or bronze. Moreover, spherical pores are preferable to elongated or sharp-edged pores. A varying pore concentration in the abrasive layer leads to changing properties such as non-uniform density. Softer zones will wear quicker and can even cause tool destruction. In addition, heat conductivity is lower in zones with higher porosity. [YARN69]

The volumetric percentage of porosity in a grinding tool can be determined by several methods:

- The porosity can be calculated from the weight of the grinding wheel compared to the theoretical weight of the pore-free tool [YARN69].
- The archimedic principle can be applied if it is assumed that all pores are hollow and connected to the surface [DAUD60]. The ascending force relates to the weight of grits and bonding. The amount of remaining air in the grinding tool can be reduced by heating of the water, slowly submerging of the tool, and adding agents that reduce surface tension [DAUD60]. This method is only useful for conventional tools.
- The surface of the pore cross-sections can be measured on photographs of the wheel [YARN69]. The quotient of pore surface area to total cross-sectional area gives the porosity. This method can be applied to superabrasive tools.

Remarkable trends in changing porosity are "ultrahigh porosity vitrified wheels" [MARI07, p. 113] resulting from long needle-shaped grits (see Sect. 4.1.2 "Special Grinding Wheel Types") and lubricated vitrified wheels (see Sect. 9.2.2 "Developments in Tool Design").

6.1.3 Secondary Grits

It is common practice to use a second type of abrasive grits, which might or might not be displayed in the tool specification. In resin bonds, secondary grits decrease bond wear. In vitrified bonds, secondary grits are fillers in the bond or take part in chip formation. Combining primary grits with secondary grits can have a synergistic effect [HAY90]. During manufacturing, secondary grits increase mold packing density [WEBS04]. Mixing different sizes of abrasive grits and bond material has the same effect.

Adding a secondary abrasive can reduce the cost of the grinding wheel, for example in the case of pricier sintered corundum [HAY90]. Secondary grits for sintered corundum can be fused alumina, co-fused alumina zirconia, SiC, BC, garnet, emery, flint, CBN, diamond, or mixtures thereof [HAY90, WEBS04]. Secondary grits for vitrified bonded CBN can be Al_2O_3 and/or SiC and work mainly as filler and support grits [LINE92, p. 39]. Corundum grits are likely to be etched by the vitrified bond [LINE92, p. 39].

6.2 Cutting Edge Density

Cutting edge density is important to understand tool performance during the grinding process. Many researchers analyzed the statistical nature of the cutting edges [KASS69, BÜTT68, SALJ88, HOU03, LORT75, etc.].

6.2.1 Definitions

6.2.1.1 Static Cutting Edge Density

Researchers differentiate between grit number and cutting edge number because each grit can have several cutting edges. However, both values are often denoted with the same letter, *N*. Grit or cutting edge distances are nominated with *L* and are approximately inversely proportional to the grit or cutting edge number, *N* (Eq. 6.4, Fig. 6.5) [SALJ88]. Important metrics are also the number of grits or cutting edges per area or per volume, often denoted with the letter C.

$$\text{Grit / cutting edge density } \mathrm{N} \sim \frac{1}{\mathrm{L}} \tag{6.4}$$

N grit/cutting edge density in [1/mm^2]
L grit/cutting edge distance in [mm]

Shaw estimated the number of active grits per unit area, or so-called approximate grain spacing, from the grit size (Eq. 6.5) [SHAW96, ROWE09]. However, Rowe stressed that wheel structure, depth of cut, and wheel deflection affect the number of active grits [ROWE09, p. 81].

$$N = \frac{1}{2.25\ d_g{}^2} \tag{6.5}$$

N grit density
d_g mean grit diameter

ISO 3002-5:1989 defines the static grit number at a certain depth, N_{st}, as the counted grit number at a certain band depth measured by a quasistationary method such as stylus, thermocouple, or microscope [ISO89]. Figure 6.4 visualizes the cutting edges emanating from the cutting area. The cutting area depth extends in normal direction to the outer tool envelope [SALJ88]. The measurement directions can be in the feed direction or perpendicular for circumferential grinding wheels and honing stones and towards the wheel center or in circumferential direction for face grinding operations [SALJ88].

The apparent contact area is the area between wheel and workpiece after Eq. 6.6 [ROWE09, p. 315]. The real contact area, however, is the sum of all contact areas on the grit tips in the respective depth of cut and much smaller that the apparent contact area (see Fig. 6.4).

$$\text{Apparent contact area } A_c = b_{seff} \cdot l_g \tag{6.6}$$

$b_{s\ eff}$ effective grinding wheel width
l_g geometric contact length (Eq. 6.7)

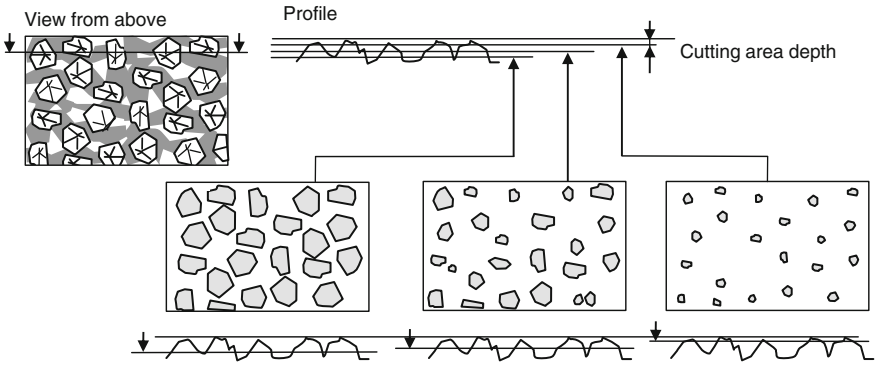

Fig. 6.4 Static grit number in different cutting area depths after [PEKL57, p. 61, SALJ88]

$$l_g = \sqrt{a_e \cdot d_{seq}} \tag{6.7}$$

l_g contact length
a_e depth of cut
d_{eq} equivalent grinding wheel diameter (Eqs. 6.15, 6.16 and 6.17)

Linke calculates the grit distance, K_{ab}, for CBN grits under the assumption of spheric grits and face centered cubic model [LINE92, p. 51 f.]. The face centered cubic model has the highest packing density of a cubic structure (74 %) [LINE92, p. 52].

$$\text{Grit distance } K_{ab} = d_g \cdot \left(\frac{\pi}{3 \cdot 2^{0.5} \cdot V_{CBN}}\right)^{\frac{1}{3}} \tag{6.8}$$

d_g grit size
V_{CBN} volumetric grit concentration in [%]

6.2.1.2 Kinematic Cutting Edge Density

Kinematic cutting edges or grits are only those of the static edges or grits engaging into the workpiece material (Fig. 6.5). The kinematic grit number, N_{kin}, can be counted at small contact forces so that the tool contact deformation is negligible [ISO89].

Equation 6.9 offers an empirical approach to calculate the number of kinematic grains per unit area, N_{kin} [WERN71]. Grit density, c_{gw}, arises from grit size, grit

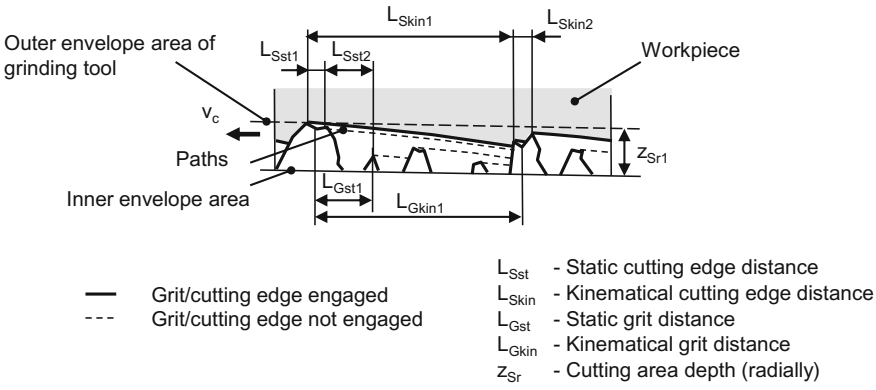

Fig. 6.5 Static and kinematic distances of grits and cutting edges at a circumferential grinding wheel [SALJ88]

shape and grit concentration. A single grit can have one or more cutting edges depending on grit shape. Yegenoglu found a formula to describe the kinematic cutting edge number in CBN grinding wheels quite accurately (Eq. 6.10) [LINE92, YEGE86].

$$N_{kin} = c_{gw}\left(\frac{v_w}{v_s}\right)^{e_1}\left(\frac{a_e}{d_{eq}}\right)^{\frac{e_1}{2}} \tag{6.9}$$

$$N_{kin} = C_1\left(\frac{V_g}{{d_g}^3}\right)^{C_2}\left(\frac{Q'_w}{q \cdot d_{eq} \cdot v_c}\right)^{C_3} \times 10^6 \tag{6.10}$$

N_{kin}	kinematic cutting edge number in [1/mm^2]
C_1, C_2, C_3	empirical constants
V_g	volumetric grit concentration
d_g	grit size
Q'_w	specific material removal rate]
q	speed ratio
d_{eq}	equivalent grinding wheel diameter
v_c	cutting speed

6.2.1.3 Active Cutting Edge Density

Furthermore, ISO 3002-5:1989 defines the active grit count, N_{act}, as grit that are actually engaged [ISO89]. Werner expressed this as number of momentary grains per unit area, N_{mom} (Eq. 6.11) [WERN71].

$$N_{mom} = \frac{1}{1+\alpha} b_s \cdot l_k \cdot N_{kin} \tag{6.11}$$

N_{mom}	number of momentary grains per unit area
α	empirical factor
b_s	wheel width
l_k	kinematic contact length
N_{kin}	kinematic cutting edges

Resin or vitrified bonded grinding wheels flatten due to wheel flexibility [ROWE09, p. 82]. Tool deflection increases contact length and number of grits (Fig. 6.6) [BORK92, ROWE09, SAIN80]. Figure 6.6 shows deformations at flat grinding; similar deformations happen during cylindrical grinding operations, with the difference that the contact zone deforms as well [PEKL57].

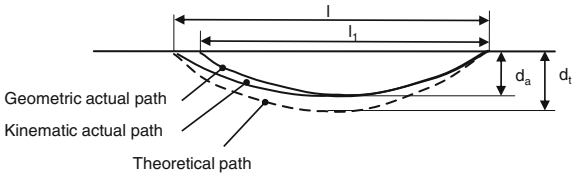

Fig. 6.6 Actual and theoretical grit engagement paths after [SAIN80], with permission from Elsevier

Grits in bonding can be viewed as a spring-damper system (Eq. 6.12) [PEKL57, p. 113]. Saini and Brown derived Eq. 6.13, where grit workpiece deflection, δ, results from actual depth of cut, d_a, and theoretical depth of cut, d_t (Fig. 6.6) [SAIN80]. Measured groove length, l, deviates from the groove length, l_1, that occurs when the workpiece stands still (workpiece speed $v_w = 0$).

$$\delta = \frac{F_{n,grit}}{c} \tag{6.12}$$

$$\delta = d_t - d_a = \frac{l^2}{4d_s}\left(\frac{v_s}{v_s + v_w}\right)^2 - d_a \tag{6.13}$$

δ	elastic grit deflection rectangular to cutting direction
$F_{n,grit}$	normal force at grit
c	spring constant of bonding
d_t	theoretical depth of cut
d_a	actual depth of cut
l	measured groove length
d_s	grinding wheel diameter
v_w	workpiece speed
v_s	wheel speed

Furthermore, workpiece speed affects the spring/damper system of grits and bond. Chip thickness per grit increases with higher workpiece speed v_{w2} (Fig. 6.7) [PEKL57, p. 113]. Higher chip thicknesses lead to higher single grit forces and larger elastic grit deviation, δ (Eq. 6.12). Therefore, the grits engage less deeply and more grits have to remove the material. In addition, the distance between cutting edges gets shorter at higher workpiece speeds [PEKL57, p. 113].

6.2.1.4 Wheel Deformation Effects

The grinding system consists of several elastic elements in series, such as motors, bearings, feed axis, spindle, grinding wheel, etc. [KING86, p. 171]. The overall stiffness, k_t, adds up reciprocally from the stiffness of each element (Eq. 6.14)

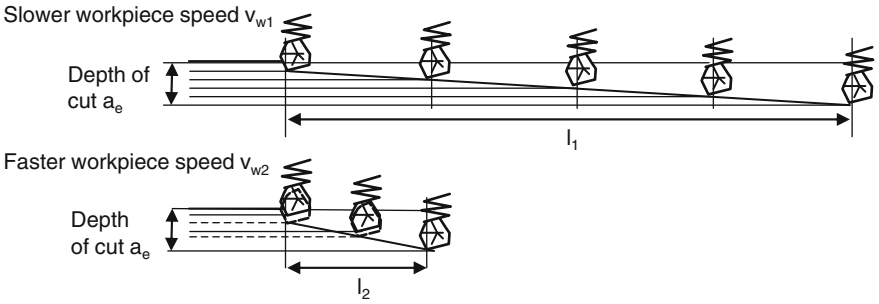

Fig. 6.7 Decrease in cutting edge distance at higher workpiece speed, v_{w2}, after [PEKL57, p. 114]

[KING86, p. 171]. The element with the lowest rigidity will dominate system rigidity.

$$\text{Inverse of total stiffness } \frac{1}{k_t} = \frac{1}{k_1} + \frac{1}{k_2} + \ldots + \frac{1}{k_i} \tag{6.14}$$

k_t total stiffness
k_i stiffness of each element in the grinding system

Geometry of the contact zone between grinding wheel and workpiece depends on the tool and workpiece diameter. To compare kinematics and engagement conditions of different grinding processes, the equivalent grinding wheel diameter is calculated from Eqs. 6.15, 6.16 and 6.17 [KLOC05a, p. 190, STEF83, p. 21].

Hahn calculates the curvature between tool and workpiece for these different cases depending on the speed ratio, q [HAHN55]. Depending on the load conditions, either the tool reproduces its own circumference (low workpiece speeds) or the curvature difference approaches the inverse of the equivalent radius [HAHN55].

$$\text{External cylindrical grinding: } d_{eq} = \frac{d_w \cdot d_s}{d_w + d_s} \tag{6.15}$$

$$\text{Internal cylindrical grinding: } d_{eq} = \frac{d_w \cdot d_s}{d_w - d_s} \tag{6.16}$$

$$\text{Surface grinding: } d_{eq} = d_s \tag{6.17}$$

d_{eq} equivalent grinding wheel diameter
d_w workpiece diameter
d_s grinding wheel diameter

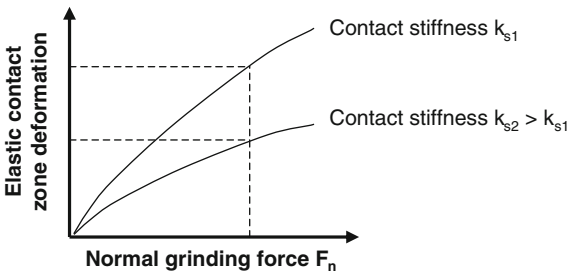

Fig. 6.8 Wheel deflection after [SCHR71]

The contact zone deformation of two touching cylinders increases with the normal forces [SCHR71, p. 40]. Higher contact stiffness leads to smaller elastic deformation (Fig. 6.8).

Gerhardt relates the grinding wheel contact stiffness to the individual grit spring constant and the preload force (Eq. 6.18) [GERH70]. The wheel stiffness can be measured by applying both a static and a dynamic force and measuring the local deformation [GERH70]. King and Hahn give Eq. 6.19 as example for a specific grinding wheel stiffness of a vitrified grinding wheel (2A60K6VLE, d_{eq} = 4.93 in. = 125.2 mm) [KING86].

$$k^* = A \cdot k^{1-b} \cdot (F'_n)^b \tag{6.18}$$

$$k^* = k_0 \cdot {d_{eq}}^{0.25} \cdot (F'_n)^{0.75} \tag{6.19}$$

k^* grinding wheel stiffness per unit width of contact zone in [lb/in.^{2}]
A constant in [1/in.]
k spring constant of individual grit in [lb/in.]
b constant depending on cutting edge distribution
F'_n normal force per unit width in [lb/in.]
k_0 constant (0.58×10^5 lb/in. ^{2})
d_{eq} equivalent grinding wheel diameter (Eqs. 6.15, 6.16 and 6.17) in [in.]

6.2.2 *Measuring, Replicating and Modeling of the Tool Topography*

Already in 1936, Goedecke emphasized that the process performance of a grinding tool depends strongly on the spacial distribution of the cutting edges [GOED36, EVER06, p. 383]. Several methods to measure, replicate and model the tool topography exist. Karpuschewski summarizes sensors and methods for measuring the grinding tool microtopography [KARP01, p. 131 ff].

6.2.2.1 Tactile Measurement

The statical cutting edge number can easily obtained by tactile measurement of the grinding wheel topography [DAUD60, p. 47 ff, PAHL68, LORT75]. However, the tactile measurement does not differentiate between grits, bonding, or chips [DAUD60, p. 48]. Stylus tip geometry affects resolution. Furthermore, the tip will be abraded by the abrasive grits. Compared to optical measurements, tactile methods are rather time consuming.

6.2.2.2 Optical and Electron Measurement Methds

Several optical measurement methods exist to analyze the actual wheel topography or topography replica. Goedecke charted replicated cutting edges with a light microscope [GOED36, EVER06, p. 383]. Stereoscopy enables obtaining three dimensional surfaces and grit shapes [DEPE05]. White stripe projection can also be used for 3D measurements. Although light scattering methods work best on a small measuring range and homogeneuous surfaces, they can be used for abrasive tools when self-shadowing phenomena are analyzed [LUKI05].

Scanning Electron Microscopy has a better resolution than light microscopical methods. Stereoscopic SEM pictures even give detailed information about abrasive layer profile and potential cutting edges [MATS75]. The disadvantage is, however, that the abrasive layer has to fit into the SEM chamber, be cleaned for the chamber vacuum, and potentially be coated with conductive gold or graphite coatings.

6.2.2.3 Other Methods

The dynamical cutting edge number results from the process kinematics and can be obtained with a thermo-element inside the machined workpiece. Each impulse during grinding should indicate a grit-workpiece contact [PEKL57, DAUD60]. The smaller the contact area of the thermo-element is, the more reliably the temperature peaks can be related to grits.

Luminescence offers another approach. Known luminescence of diamonds for X-rays allows to measure number and size of free-standing diamond grits in a resin bonded diamond wheel after it has been irradiated with focussed X-rays [TOML78a].

6.2.2.4 Replica Methods

The grinding wheel topography itself exhibits some challenges to most measurement methods, such as reflectivity, transparency of grits, or abrasiveness. Therefore, the abrasive layer topography is replicated, but the reproduction quality has to be considered. A simple method is to press a plain paper and a carbon paper onto the

wheel surface [GOED36, LORT75]. Every blackened area can be interpreted as cutting edge.

Another method by Nakayama and Shaw works with grinding in an inclined polished plate [NAKA66, KÖNI70]. Through plate inclination, the grit density in different depths can be obtained. Grinding wheel topography can also be copied onto a workpiece, if workpiece rotations and grinding wheel rotations are coupled with an integer value [PAHL68].

6.2.2.5 Modeling

Several researchers have been working on describing the cutting edge shape because this knowledge is crucial for modeling of wheel and workpiece topography [DOMA06]. Cubes, spheres, ellipses, or octahedrons are common approximations for grit shapes.

Much research has been done on kinematical-geometrical models, where the grinding wheel topography engages with the workpiece. Heinzel, Brinksmeier et al. [HEIN09b, BRIN06] give a broad overview on the state-of-the-art. Kassen [KASS69] did 2D computer simulation. Today 3D simulations help to understand generated surfaces [KOSH03]. New research uses randomly shaped and distributed polyhedrons as grits, which is particularly suited for porous wheels [ZHAG11].

6.3 Tool Wear Effects

Tool wear is an important factor of grinding tool performance. Already in 1914, Alden proved that a larger depth of cut causes greater tool wear [MALK68, ALDE14]. Tool wear can be split into macro effects (tool profile loss) and micro effects (sharpness loss). Marinescu et al. [MARI07] add roundness deviation as performance characteristic to profile and sharpness loss.

6.3.1 Macro Effect—Tool Profile Loss

Dimensional wear at the grinding tool leads to a loss in workpiece dimension and profile. Cylindrical abrasive layers wear at the radius and at the edges, so that both wear volumes define the dressing allowance to retrieve the original tool profile (Fig. 6.9). Corner wear [MALK08] is also known as edge wear [KLOC09]; radius wear [WERN73] is called radial wear [KLOC09] or uniform wear [MALK08].

Werner explains that both wear effects are induced by similar process characteristics, which are average single grit cutting force, friction speed, contact time, and contact frequency [WERN73, p. 69]. At tool corners, grit support within the abrasive layer is weaker, so wear rate is faster [WERN73, p. 69]. During each wheel

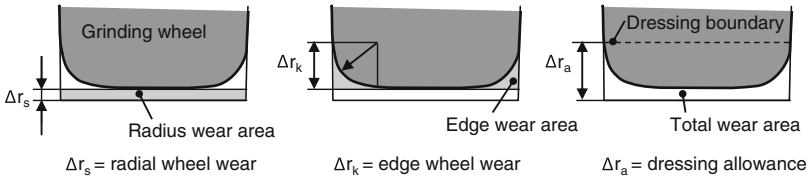

Fig. 6.9 Radius wear and edge wear at a plunge grinding wheel [WERN73, p. 70]

rotation, the grinding forces are more likely to overload the weaker bond bridges at the wheel edges until an equilibrium between grit retention forces and grinding forces is achieved [BIER76, p. 77 ff]. In external cylindrical plunge grinding, the edge wear appears with an elliptical contour [WEIN76, BIER76, p. 77 ff]. Circular edge profiles occur only for small material removal rates or short process times [BIER76].

König and Henn [KÖNI84] explained the wear behavior of grinding wheels in centerless throughfeed grinding or other traverse grinding operations (Fig. 6.10). The grinding wheel can be divided in parts being as wide as the workpiece feed per wheel revolution. Every part has to remove a certain amount of workpiece volume. Due to inevitable wear, each part cannot remove as much material as originally intended, causing higher work load for the following part. This results in even more wear at the next parts until the spark-out zone of the grinding wheel is reached, where originally no material removal took place. The spark-out zone works as buffer and takes over some part of grinding of the workpiece allowance. Decreasing spark-out zone width leads to decreasing overlap ratio and increasing workpiece roughness. If the whole spark-out zone is worn, the workpiece dimension will deviate [KÖNI84].

Load direction, e.g. defined by feed direction, affects the wear profile (Fig. 6.11). Furthermore, similar profile wear behavior exists at other tool types. Büttner

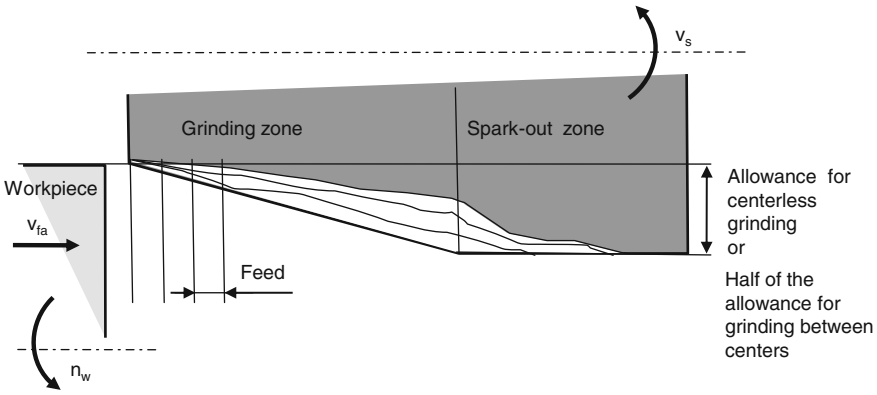

Fig. 6.10 Profile wear in longitudinal grinding [KÖNI84]

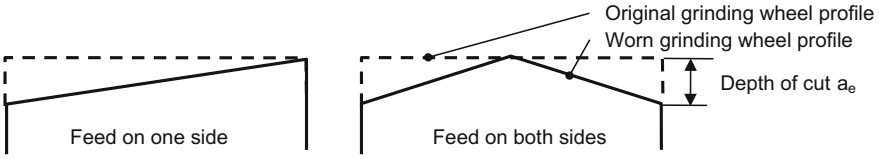

Fig. 6.11 Wear in different profiles or paths [METZ86, p. 68]

[BÜTT68, p. 64 f.] for example examined the formation of main wear area and side wear area at cup grinding wheels.

6.3.1.1 Wear Measurement

In most industrial applications, wheel wear is assumed from workpiece profile deviations. In research settings, wheel wear is commonly determined by reproducing the rotating grinding wheel into a steel plate. The grinding wheel needs an unworn reference part such as a part of the abrasive layer that did not interact with the workpiece. Karpuschewski [KARP01, p. 126 ff] gives an overview about sensors for measuring the macroscopic profile of grinding tools.

6.3.2 Micro Effect—Sharpness Loss

High initial tool wear is observed after dressing or for a new tool; then a steady-state tool wear follows [JACK11, p. 50, 92, BUTT79]. Wheel collapse occurs as third wear phenomena presumably because of wheel dulling and high grinding forces [BADG09b]. The dressing process affects the initial wear dominantly, whereas the steady-state wear is dominated by the grinding process conditions. The reasons for sharpness loss are explained in Sect. 6.4 "Tool Wear Mechanisms".

Loss of wheel sharpness, or dulling, leads to a change in surface roughness and higher process energy, which bears the risk of thermal workpiece damage. Excessive wear with large volume grit breakout reduces grinding forces and enlarges surface roughness, but dimensions are hard to keep and the shorter wheel life increases tool costs. A balance between self-sharpening and wheel costs is favored. For example, high performance processes need a grinding tool with high grit retention over a longer period [BAIL02]. Precision parts need high surface quality and high process stability, which is commonly accomplished through shorter dressing intervals.

Dressing restores tool sharpness and profile (see Sect. 6.5 "Tool Conditioning"). Multi-layered superabrasive tools enable longer intervals between dressing operations than conventional tools (Fig. 6.12). Single-layered tools show an initial wear

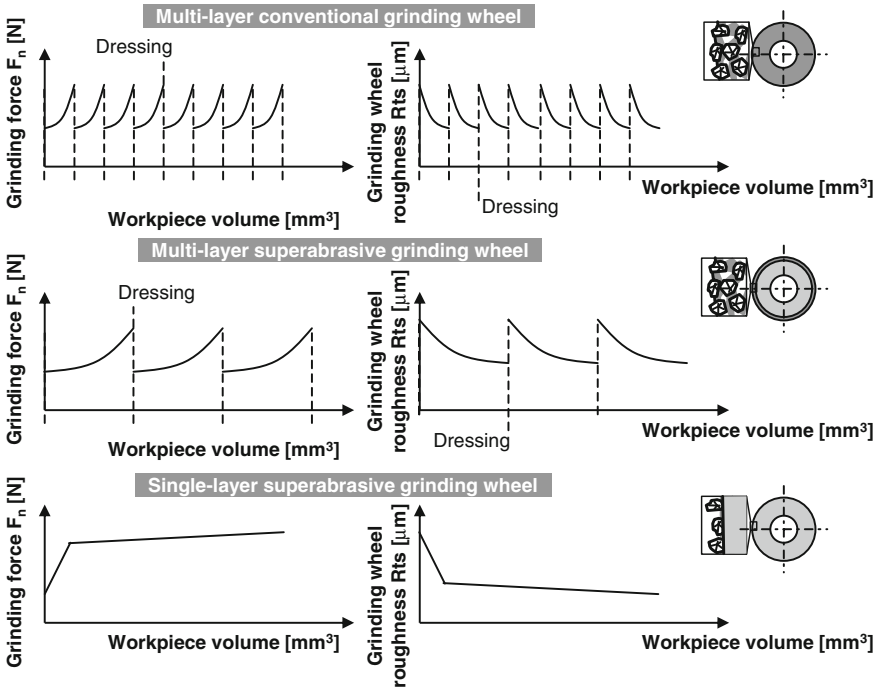

Fig. 6.12 Example wear behavior of different grinding wheel types

phase followed by quasi-stationary behavior until the tool's end of life defined by thermal damage to the workpiece [KLOC09]. Single-layered tools are not profiled or sharpened in the common sense, although sometimes so-called touch-dressing is applied to level protruding edges.

6.3.3 G-Ratio

Tool life between conditioning is measured in time, per number of machined workpieces or workpiece volume removal [PAUC08, p. 343]. The G-ratio is a common parameter for describing the tool lifespan as ratio of machined workpiece volume, V_w, and worn grinding tool volume, V_s (Eq. 6.20) [MALK08]. The G-ratio depends on the machined material, tool design, grinding operation and parameters, cooling lubricant, machine tool, etc. Therefore, no certain value can be given for a generic application, but literature provides ranges of G-ratios (e.g. Table 6.1 or [PAUC08, p. 350]). In addition, tool suppliers have databases on case studies (Fig. 6.13).

In precision grinding of steel, maximum values for the G-ratio of about 50 mm^3/mm^3 can be reached with alumina wheels and G-ratios of more than 10,000 mm^3/mm^3 with CBN wheels [HELL05a]. In contrast, a G-ratio of

Table 6.1 Typical G-ratios or relative wear resistance values for grain types [JACK11, p. 9 f.]

	Grinding alumina	Grinding steel	Grinding nickel	Grinding titanium
Diamond (9000 HV)	100,000	1000	100	500
CBN (4500 HV)	1000	10,000	5000	100
Alox (1800 HV)	<1	5–10	10	1
SiC (2800 HV)	10	1–5	1	10

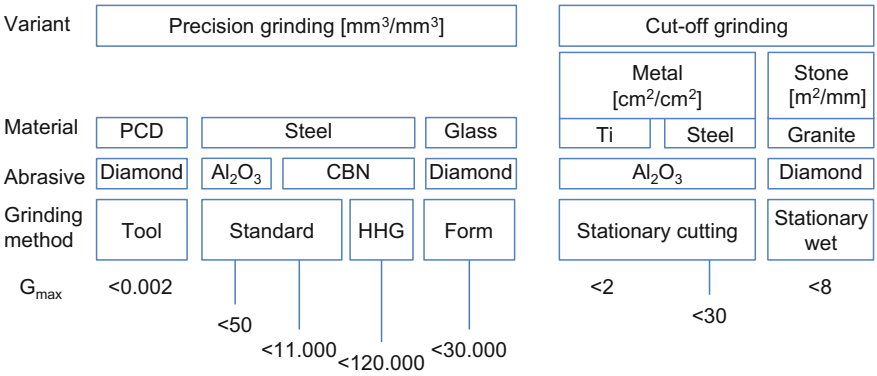

Fig. 6.13 Maximum values for G-ratios [HELL05a]

0.02 mm^3/mm^3 represents an excellent value for precision grinding of polycrystalline diamond with diamond wheels [HELL05a].

$$\text{G}-\text{ratio } G = \frac{V_w}{V_s} \tag{6.20}$$

V_w workpiece volume
V_s grinding wheel volume

The highly complex and multivariant grinding setup complicates modeling of the wear rate, although Werner claims that the high number of simultaneous grit engagements decouple the process results from the failure of a single cutting edge [WERN73, p. 67]. A wear rate model is necessary for calculating waste streams and tool costs.

Decneut et al. [DECN74] relate the G-ratio to the equivalent chip thickness, h_{eq} (Eq. 7.9), with charts. Werner [WERN73, p. 80 ff] built a wear model by multiplicative superposition. He included the four wear criteria of contact pressure,

friction velocity, engagement time, and engagement frequency and derived Eq. 6.21 [WERN73, p. 90]. Factor P includes the grinding wheel diameter, cutting edge density and edge shape factor and was derived through experimental tests [WERN73].

$$W = P \cdot (v_w)^{2m-h} \cdot (v_s)^{h+i-e-2m} \cdot (a_e)^{\frac{e}{2}+m-h} \cdot \left(\frac{d_w}{d_w \pm d_s}\right)^{\frac{e}{2}-m} \cdot (d_s)^{\frac{e}{2}-m-h} \cdot (V'_w)^h \tag{6.21}$$

W	wear cross-sectional area
P	linear factor from grinding wheel specifications in [mm^2/mm*kp]
e, h, i, m	system constants ($0.5 < m < 1.5$; $0.5 < i < 1.0$)
V'_w	specific workpiece volume [mm^3/mm]

Bierlich [BIER76, p. 83] derived the tool life volume, V'_{stand}, between two dressing operations in Eq. 6.22. This criterium can be integrated easily as cost function. Osterhaus [OSTE94] combined regression models of wheel wear in cylindrical and surface grinding processes.

$$V'_{stand} = C_4 (Q'_w)^{\alpha_4} (v_s)^{\beta_4} \tag{6.22}$$

V'_{stand}	tool life volume per mm wheel width
C_4, α_4, β_4	constants
Q'_w	specific material removal rate
v_s	wheel speed

G-Ratio and maximum material removal rate are often contradictory, so Helletsberger proposes to regard the performance factor, *L*, as factor from G-ratio and specific material removal rate, Q'_w, (Eq. 6.23) [HELL05a]

$$\text{Performance factor } L = G \cdot Q'_w \tag{6.23}$$

G	G-ratio
Q'_w	specific material removal rate

Interrupted cuts increase the number of entry and exit impacts on the grinding tool leading to higher tool wear, so that uninterrupted cuts are preferable [METZ86, p. 78 ff].

Literature mostly disregards that tools can have the same G-ratio but with different machined workpiece volume, such as $G = V_w/V_s = 10/0.1 = 500/5 = 2000/20 = 100$. If the same G-ratio is achieved in the same time, the tool performance varies greatly. Figure 6.14 shows an example where the grinding forces propagate differently and the dressing intervals vary, although the G-ratio is similar. Although high G-ratio is

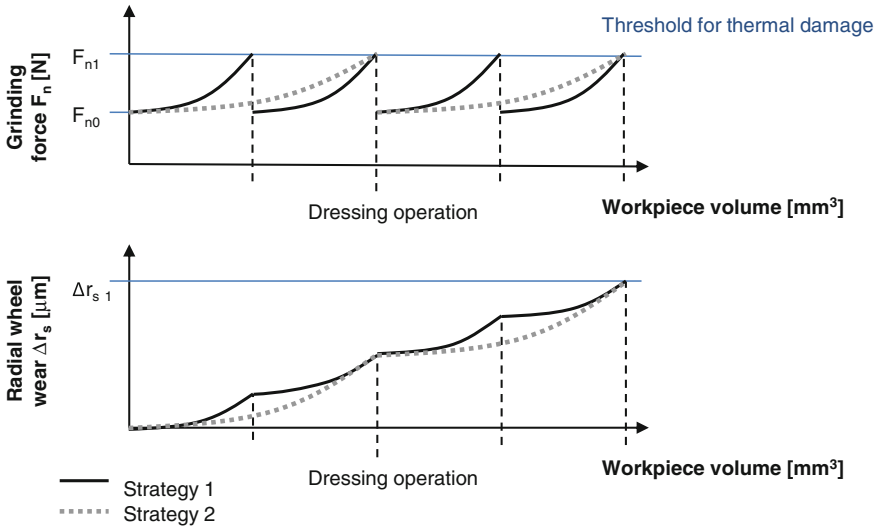

Fig. 6.14 Different grinding forces for dressing strategies with similar G-ratio

desirable, a highly wear-resistant tool may generate higher forces and grinding energies, thus increasing the potential of thermal workpiece damage.

6.4 Tool Wear Mechanisms

Abrasive machining processes themselves can be regarded as tribological systems where workpiece material and abrasive tool interact under the influence of cooling lubricant and atmosphere [MARI04]. Abrasive tools are subjected to high temperatures and high pressures in the active cutting zone. Consequently, tool wear occurs. Tool wear happens because of mechanical effects (vibrations and grinding forces), chemical effects (reactions with cooling lubricant and workpiece material), and thermal effects (grinding pressure and friction) [BOLD02, KLOC09, p. 15].

6.4.1 Wear Types

Like in all tribological systems, the wear mechanisms do not appear in single but occur as superposition or sequence [HABI80]. The tribological definition of wear is that particles are removed from the surface of one friction partner under the conditions of the surrounding environment, such as lubricant and atmosphere, and friction parameters, such as pressure, friction speed, temperatures.

Table 6.2 Taxonomy and types of wear mechanisms in the literature

	Grit surface layer wear	Grit splintering	Grit-bond-interface wear	Bond wear
[KLOC09]	Compressive softening, chemical wear, abrasion	Micro-breakage, grit breakage		Bonding breakage, chemical and thermal wear of bonding
[KÖNI81]	Abrasion, micro-cracks, corrosion, diffusion	Micro-fracture, grain fracture		Bond fracture, chemical bond wear
[MALK08, MALK68]	Attritious wear	Grain fracture		Bond fracture
[JACK11]	Abrasive wear (surface flats)	Fracture of abrasive grains	Fracture at interface grit/bond	Fracture of bond bridges
[BORK92]	Attrition, surface microchipping	Grain chipping and cracking	Grit pull-out	Bonding bridge failure
[ROWE09]	Rubbing	Grain micro- and macro fracture	Grain pull-out	Bond fracture
[PEKL58]	Compressive softening	Splintering of crystal clusters, partial grit break-out	Total grit break-out	

Different researchers use various terms for tool wear (Table 6.2), but the main categories are wear of the grit surface, wear of the grit by splintering, wear of the grit-bond-interface, and wear of the bond. The wear mechanisms of grinding tools leading to profile and sharpness loss as explained in Sect. 6.3 are complex.

Peklenik [PEKL57] highlights the alternating temperature load on the grits, because every grit contact heats up the workpiece surface on a small contact area and the grits are cooled down by the cooling lubricant (Fig. 6.15).

The wheel hardness is an important impact factor on the wear phenomena [STET74]. Softer wheels show higher wear rate, but can also be longer in a sharp

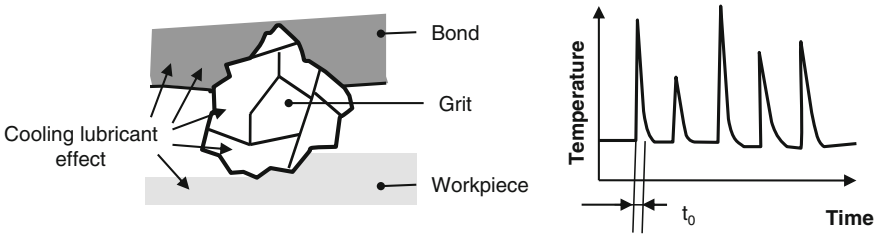

Fig. 6.15 Load at a single grit, *left*: Cooling effect by the cooling lubricant, *right*: Peak temperatures during grit engagements of intervals, t_0 [PEKL57, p. 88]

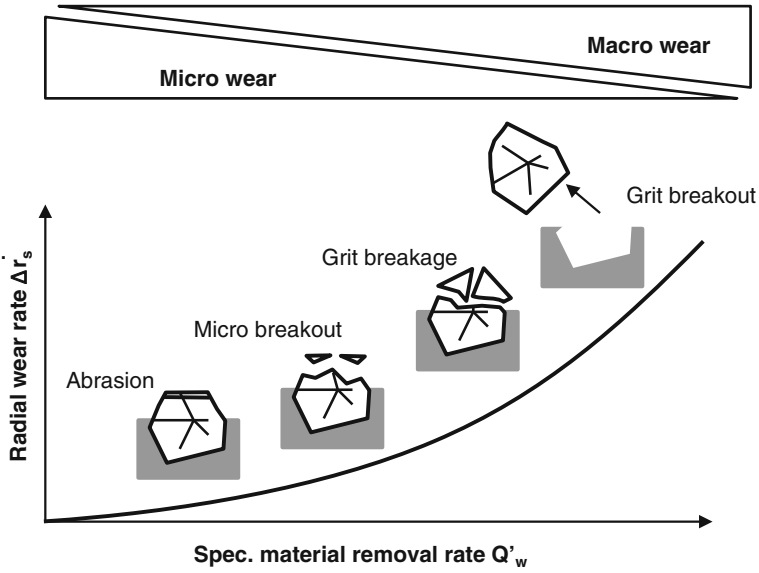

Fig. 6.16 Influence of material removal rate on wear phenomena [KLOC09, p. 254, BIER76], with kind permission from Springer Science + Business Media

cutting state [STET74]. In addition, the process parameters affect also the wear phenomena. For example, higher specific material removal rates result in higher single grit loads, which change the wear mechanism from abrasion to particle break-out and total grit break-out (Fig. 6.16). The different wear phenomena then result in different amounts of wheel profile loss [STET74].

The grit type affects how the grits get dull. For example, green silicon carbide and white aluminum oxide are friable and offer new cutting edges easily [PAUC08, p. 346]. Regular aluminum oxide acts comparatively tough and gets blunt [PAUC08, p. 346].

One way to analyze the wear phenomena is to collect the grinding debris from the grinding zone, wash the debris in benzene and separate the metallic chips magnetically [STET74]. The chips can be weighted and compared to the sieved and weighted wheel wear particles.

6.4.2 Grit Surface Wear

Malkin defines attritious wear referring to the development and growth of wear flats on the tips of active grains. Attritious wear is measured by the percentage of the wheel surface covered with wear flats [MALK68, p. 36]. Jackson defines attritious wear as wear that occurs “atom by atom” by physical and chemical interaction

between grain and workpiece [JACK11, p. 8]. Several wear mechanisms are responsible. Surface shattering, fatigue, and softening result from the basic wear mechanisms explained in the following.

6.4.2.1 Abrasion

Abrasion occurs when roughness peaks of a counter-body or particles in a medium penetrate the body's surface and perform a movement parallel to the surface simultaneously. This leads to formation of grooves and micro chips [HABI80, RABI95]. The extreme grinding pressures and temperatures initiate oxidation and diffusion processes in the grit surface layers, which decrease the abrasion resistance of the grit material [KLOC05a].

Abrasion occurs differently at ductile and brittle materials. Brittle materials wear by particle breakouts [HABI80]. Anisotropic materials such as diamond have different resistances against abrasion in their different crystallographic planes. Abrasion at diamonds is a micro fracture process. Micro cracks spread in the loaded zone and atom bonds break due to stress accumulation [SEN91, WILK91]. Micro fracture processes occur mostly along octaheder planes because there are less atom bonds to break than along the other planes [WILK62]. The border between abrasion and breakage as failure mechanisms is hard to define.

Minke [MINK88] found groove marks on dressing diamonds which gave the impression that the diamonds were scratched by softer corundum grits. This effect is explained by temperature related hardness decrease of the counter parts. The thermal stability limit of diamond (about 700 °C) is attained earlier than the one of corundum (about 1160 °C).

Ludewig [LUDE94, p. 61 ff] derives that plastic deformation of corundum grits is possible. The grinding temperatures of 1400 °C lead to a decrease in toughness (about 40 % of toughness left compared to 25 °C). In this region, the bearable compressive stresses of corundum are met during the grinding of hardened steels.

6.4.2.2 Adhesion

The direct contact of body and counter body can lead to atomic bonds ("micro weldings"), which are defined as adhesion [GAHR87, RABI95]. A relative movement of the contact partners does not necessarily involve that the bonds break within the original contact areas, so that material transfer can happen [HABI80].

Adhesive layers change the friction conditions. When steel components are ground with diamond wheels, built-up edges are formed on the diamond grits. They are mainly caused by the adhesion of steel particles on the diamond and not by welding processes of chips with the bonding [LINB70].

Focussed Ion Beam (FIB) separation allows damage free cutting of material samples out of the surface layer with electron transparency. Engelhorn [ENGE02, p. 90] found adhesive layers on sol-gel corundum grits after single grit scratch tests.

Supposedly, the nanocrystalline layer was molten and in a highly viscous state during grit engagement, so that friction and wear were reduced. Zeppenfeld [ZEPP05] found adhesive layers on diamond grits after scratch tests at γ-titanium aluminide and identified the layers as workpiece material via Electron Beam Microanalysis (EBMA). Werner also discussed the wear minimizing effect of tribo-layers with cooling lubricant, but pointed out that the adhesive layers will wear also at some point [WERN73, p. 79].

6.4.2.3 Tribochemical Reaction

Tribochemical wear is the most complex wear mechanism [MARI04, RABI95]. It includes a reaction between body, counter body and environment [DIN79, HABI80]. A large reactive surface or friction heat accelerate these reactions.

Beads of molten workpiece material give evidence of the high temperatures during the cutting action. For example, Müller [MÜLL01, p. 57] found beads of molten workpiece material (bearing steel) on SiC grits after single grit scratch tests. Reactions of the workpiece surface, the grit or bond material are promoted by grinding process heat. Possible reactions of the abrasive grits were explained in Chap. 2 “Abrasives”.

6.4.3 Grit Splintering or Breakage

In brittle materials, such as grit materials, it is hard to differentiate between microscopic breakage processes, or wear by abrasion [WILK91]. This is because the grooves and small chips, which generally help to detect abrasion, are missing in brittle materials due to their low tensile yield point [WILK91].

In monocrystalline diamonds, breakage occurs along the cleavage planes. Polycrystalline diamonds break along the crystal boundaries. Wear by micro-chipping occurs at friable diamond [BAIL99]. When machining hard, brittle, short chipping workpiece materials with the more friable diamonds, the grinding forces tend to be lower and surface roughness smaller [BAIL99].

Alternating thermal or mechanical load lead to elastic and plastic deformation, change of material hardness (softening or hardening), crack formation and crack propagation [GAHR87, RABI95, PEKL57, p. 86 ff]]. Surface shattering is a fatigue mechanism occuring at impact load [DIN79, HABI80]. Grain boundaries or cleavage planes open and the cracks start at or near the surface [GAHR87].

6.4.4 Grit-Bond-Interface Wear

For **resin bonded grinding tools** grit break-out is the main wear mechanism and, therefore, the grit holding forces within the bond are essential for tool wear [TOML76]. Abrasive particles worn more than 50 % of their diameter are not likely to retain in the bond any more. Moreover, there are details in the literature that not even 35 % of blocky grits can be used in the machining process before break-out [TOML76].

However, abrasives to be used in resin bonds should have high surface roughness and irregular shapes to have high bond adherence. Often metallic coatings optimise the retention of superabrasives by providing even rougher surfaces and possible chemical reactions to the bond additional the mechanical clamping.

Büttner found that diamond grits in resin bonding showed more grit break-outs than grits in bronze bonding, which were held more strongly and showed attritious wear [BÜTT68, p. 72].

6.4.5 Bond Wear

Several chemical reactions can happen at the wheel bonding [BRIN04]. There Brinksmeier and Walter found chemical reactions of the fillers in a resin bonded corundum wheel with the cooling lubricant additive [BRIN00].

In many cases, grit wear leads indirectly to mechanical bond wear. Worn and flattened cutting edges expose an enlarged friction surface, which leads to an increase in cutting forces on the individual grit. Consequently, the bond can be mechanically overloaded and entire grits or grit sections can break out of the bond [KLOC05a].

6.4.6 Clogging of the Abrasive Layer

Clogging or loading of the abrasive layer describes the adhesion of chips to the abrasive grits or interlocking of chips in the pore space. With more wheel clogging, the danger of thermally induced damage of the workpiece surface layer, the workpiece roughness and the grinding wheel wear rise [LAUE79]. Lauer-Schmaltz [LAUE79] pointed out that the effect of grinding wheel loading depends not only on the particle spacial size, but furthermore on the particle positioning within the abrasive surface layer.

Lauer-Schmaltz [LAUE80] and Koenig defined three loading types: Chip nests, welded chips, and grit adhesions:

- Chip nests or clustered chips are long, solitary chips in front of active cutting edges [LAUE79]. This type of loading results from mechanical clustering of

chips in the neighbored pores of active grains and does not necessarily disturb the grinding process.

- Welded chips consist of pressure welded chips and adhere, in contrary, on the active cutting edge and, thus, increase the effective cutting edge radius. As consequence, the single grit chip thickness increases. Lauer-Schmaltz [LAUE79] found areas up to 2 mm^2 of the grinding wheels covered.
- Grit adhesions cover groups of grits thinly and do not impair the cutting edge shape, but only the friction properties at the flanks [LAUE79]. This type of loading was examined during the machining of chromium and nickel containing materials as well as titanium and aluminium alloys. There can be chemical reactions in the boundary layer between chips and active grains [LAUE80].

Wheel loading depends on the machined material. Pai et al. [PAI89] compared chips from grinding ductile and brittle materials and found that the chips tend to be longer in ductile machining. These longer chips can cause clogging problems of the grinding tool. In comparison, brittle materials tend to exhibit a smaller chip storage problem than ductile materials and hence allow a greater removal rate for the same available chip storage volume [PAI89].

Nagaraj and Chattopadhyay [NAGA89] concluded that chemical reactions have an effect on loading, for example, iron oxide layers are formed on machined C45 steel and prevent adhesion to the abrasive grits. Titanium alloys in contrast might form strong bonds to the corundum grits and form adhesions [NAGA89]. Pure iron led to a relatively high wear rate because of its high ductility and, consequently, chip layers [LUDE94, p. 89 ff]. Furthermore, steels with abrasive Zementit particles in a soft Ferrite matrix like C135 W induced wear due to loading [LUDE94, p. 92]. On the one hand, the Zementit crystals were pushed into the softer matrix and caused minor abrasion. On the other hand, adhesions of workpiece material on the grits resulted in high tangential forces and grit particle break-out.

Normalized steels with higher carbon content lead to less overall wear, because the increasing Perlit content decreases clogging [LUDE94, p. 93]. Nevertheless, the Zementit lamellas of the Perlit cause wear by abrasion, but to a minor proportion compared to the wear by adhesions.

To grind highly ductile material like pure iron, a grinding tool with open pores and low bond strength is advantageous, so that loaded abrasive cutting edges can break out off the abrasive layer [LUDE94, p. 102]. With higher possible material removal rate, higher grinding wheel wear goes along.

There are approaches to monitor grinding wheel wear and loading via CCD camera images [ARUN07, HEIN12]. Various texture analysis methods such as variance, energy, ASM, diagonal moment, IDM, and Ga parameter can be used to characterize texture changes, which are related to the grinding wheel surface condition. However, it is difficult to assure constant measurement conditions, such as illumination. The analysis for each grinding wheel and workpiece material has to be calibrated [ARUN07].

6.5 Tool Conditioning

6.5.1 Overview on Conditioning Principles

Grinding wheel topography is influenced by grinding wheel structure, profiling and sharpening process as well as by the wear during the use of the grinding wheel [MARI04]. The dressing process changes the working behavior of the grinding tool, the Young's modulus and the effective hardness of the grinding layer [MARI04]. In addition, the abrasive layer will change during the grinding process [STUF96]. The dressing process should enable a grinding process as consistent as possible considering grinding wheel wear.

Abrasive tools are prepared for use to be set up for a new grinding application according to profile and micro topography, to true their roundness deviation and to compensate their wear. The term "dressing" envelopes the processes of "profiling" or "truing", i.e. the generation of the demanded grinding tool profile, and "sharpening", i.e. the generation of cutting ability [KLOC05a, SPUR89, TÖNS04]. Sometimes "dressing" refers only to sharpening. Depending on abrasive tool specification and machine set-up, profiling and sharpening have to conducted as separate processes. In general, dressing consumes a lot of grinding wheel volume [STET74], sometimes up to 90 % of the grinding wheel volume.

The various dressing methods can be organized by different criteria, such as active medium, active principle, or process kinematics [HESS03, KLOC05a, SPUR89, LINK07]. Active dressing media can be with or without diamond. Active principles are cutting of grits and bond, setting back the bond, or removing the bond. To set back the bond, diamond free tools like steel rollers, silicon carbide wheels, or sharpening tools of bonded abrasives are used. Material removal processes are restricted to metallic bonds and work with electro-chemical or electro discharge processes [SPUR89]. In laser conditioning, bonding is vaporized before the abrasive grits are harmed [SHAW96]. Laser assisted dressing is a hybride procedure. The laser beam softens vitrified bonding to support dressing with diamond tools [ZHAN03]. Sand blasting is used for bond sharpening at honing sticks. The applied dressing strategy always depends on quality and cost requirements and the available machine concept. Wegener et al. [WEGE11] give a detailed overview on profiling and sharpening strategies.

6.5.2 Dressing with Diamond Tools

Today, dressing tools with diamond material are commonly used for grinding wheels [KLOC05a], using either stationary or rotating dressing tools. Stationary tools move parallel along to the grinding wheel axis on a path defined via NC

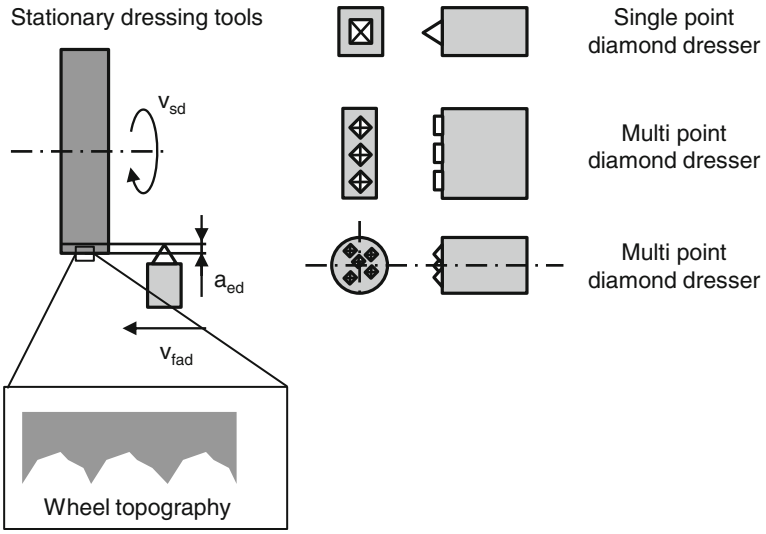

Fig. 6.17 Stationary dressing tools

programming or guide ruler (Fig. 6.17). The grinding wheel topography is generated like in a turning process [KLOC05a]. The stationary dressing tools consist of one or more diamond grits or synthetic diamond logs in metallic bond. Single grit dressers often are made of profiled natural diamonds of high purity, which can be re-positioned when worn. Diamond splinters or synthetic logs are often utilised in multi-grain dressers or dresser tiles.

Rotating dressing tools have an additional movement in circumferential direction of the grinding tool and provide a layer of diamonds along their perimeter (Fig. 6.18). The larger diamond volume of rotating tools improves wear resistance and profile retainability and, therefore, leads to higher dressing process stability [FALK98, WARN88].

Rotating tools are form rollers, profile rollers, or cup disc dressers. Form rollers and cup dressers have an axial feed rate along the grinding wheel axis, whereas profile rollers display the grinding wheel negative profile and are fed radially towards the grinding tool. Form rollers can be used flexibly for different profiles, while profile rollers are limited to one application [HARB97, KLOC87, SALJ84]. Wear formation at a form roller effects not only contour accuracy but also abrasive layer topography because of the changing effective dressing width [SALJ84]. With appropriate wear monitoring these effects can be compensated. However, profile wear at profile rollers leads inevitably to tool life end.

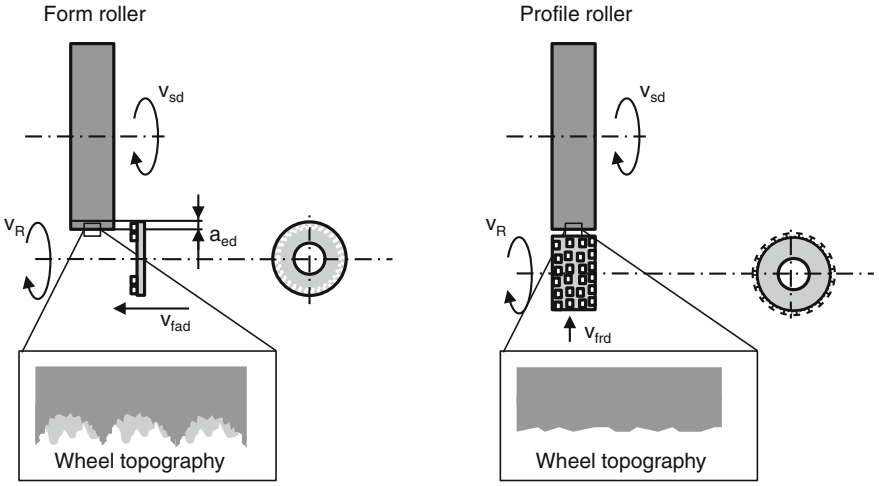

Fig. 6.18 Rotating dressing tools

6.5.3 *Dressing Parameters*

6.5.3.1 Overlap Ratio

Overlap ratio, U_d, is an important metric for dressing processes with axial feed rate [SALJ84]. It indicates how frequently the dressing tool overtravels a point on the grinding wheel. Overlap ratio is calculated from engagement width of the dressing tool, a_{pd}, and axial feed per grinding wheel revolution, f_{ad} (Eq. 6.24).

$$U_d = \frac{a_{pd}}{f_{ad}} \tag{6.24}$$

$$\text{with } a_{pd} = \frac{b_d + f_{ad}}{2} \tag{6.25}$$

a_{pd} engagement width
f_{ad} axial feed
b_d active dressing tool width

For inclined contour elements of the grinding wheel profile, the overlap ratio can be calculated for the direction of the contour, axial, or radial direction [HARB97]. For cylindrical dressing tools and in most industrial applications the simplified Eq. 6.26 is used [KLOC05a, VDI04]. Active dressing tool width, b_d, depends on the depth of dressing cut, a_{ed}.

$$U_d = \frac{b_d}{f_{ad}} \tag{6.26}$$

b_d active dressing tool width
f_{ad} axial feed

Small dressing feed or high overlap ratio results in grinding wheel topography with small active surface roughness, low grit protrusion, and a high number of kinematic cutting edges [KLOC05a, MARI04, SCHU96, STUF96]. The favorable small part surface roughness is accompanied by the danger of higher grinding forces and stronger grinding wheel loading. Therefore, grinding wheels for roughing operations are dressed with small overlap ratios.

Workpiece surface roughness decreases with increasing overlap ratio, so that a maximum overlap ratio exists above which the part surface roughness cannot be improved significantly. Messer [MESS83] found a maximum value, U_{dmax}, in empirical tests, which depends on grinding grit size (Eq. 6.27).

$$U_{dmax} = \frac{\text{grit size in US Mesh}}{15} \tag{6.27}$$

6.5.3.2 Depth of Dressing Cut

For stationary dressers and form rollers, depth of dressing cut, a_{ed}, defines engagement depth of the dressing diamonds with the grinding tool in normal direction. For profile rollers radial dressing feed, f_{rd}, has the same implication.

Grinding wheel wear and grit size define the depth of dressing cut [AVER82]. The depth of dressing cut should be smaller than grit size to ensure that the grinding tool structure stays connected [MARI04]. One strategy is to conduct final dressing strokes with no depth of cut, so that the elastic deformations between grinding wheel and dressing tool are leveled out and the wheel topography is smoothened [MALK08, MARI04, SHAW96]. The same effect takes place if profile rollers are kept rotating at the end of the dressing process without further radial infeed.

The influence of depth of dressing cut is not homogeneous in the literature. Messer, Marinescu et al. found an increase of the theoretical effective grinding wheel roughness increases slightly with the depth of dressing cut [MARI04, MESS83]. Inasaki [INAS77] obtained that the workpiece roughness increases degressively. Larger depth of dressing cut leads to more splintering of abrasive grits [STUF96] and to shorter instationary wear phase of the grinding tool [SCHU96].

6.5.3.3 Dressing Speed Ratio

Dressing speed ratio, q_d, gives the ratio between dressing roller speed and wheel speed (Eq. 6.28). In up-dressing, the speed vectors are counter-directional in the contact point and the speed ratio is denoted with a negative value; in down-dressing everything is inverted.

$$q_d = \pm \frac{v_R}{v_s} \tag{6.28}$$

v_R dressing roller speed
v_s wheel speed

Dressing speed defines the engagement curves of dressing diamonds into the grinding wheel [SCHU96]. The rotations of dressing roller and grinding wheel superpose, so that the dressing diamonds move along cycloidic paths viewed from the grinding wheel [SCHE73]. Dressing diamond paths for down-dressing have steeper flanks for the same value of the speed ratio in up-dressing, $/q_d/$ [SCHM68]. Therefore, rougher grinding wheel topography results. Contact length between dressing diamond and grinding wheel decreases with increasing value of the speed ratio, $/q_d/$, and the engagement angle gets steeper [STUF96]. This affects the wear mechanisms of the abrasive grits. Grits dressed in down-dressing mode splinter and break more, whereas grits dressed in up-dressing are rather flattened [STUF96]. At the dressing speed ratio of $q_d = +1$ grinding and dressing tool move with the same speed and high normal forces occur. The grinding layer is shattered by high normal forces and the dressing principle is called "Crushing" [HESS03]. Special brittle bond systems work best for crushing, for example brittle bronze bonding.

Experiments have shown that not only the dressing speed ratio, but also the relative speed between dressing roller and grinding wheel are important.

6.5.3.4 Dressing Mechanisms

During dressing with diamond tools, the active mechanisms are grit breakage and splintering, bonding breakage, grit break-out of the bonding, and grit deformation [MARI04, WIMM95, MINK88, MESS83, KLOC08b]. For vitrified bonded wheels, dressing forces seem to have a crucial effect on the disruption of the abrasive layer and therefore on the wear behavior after dressing [LINK07].

Çinar [CINA95] developed a grit collision model to describe mechanisms in cup dressing and predict workpiece surface roughness. Linke [LINK07] extended the model to other dressing tool types and combined it with a dressing force model.

The initial grinding wheel wear after dressing can be high, before the wheel wear gets into a steady state that is defined by the grinding process conditions only (see Sect. 6.3.2 "Micro Effect—Sharpness Loss"). In industrial practice, the grinding wheel wear often is compensated with a few dressing strokes with a high depth of

dressing cut followed by a last stroke with a smaller depth of dressing cut to reduce the grinding wheel surface roughness. However, grinding wheel scratch tests verified that a higher depth of dressing cut and a smaller dressing overlap ratio disrupt the abrasive layer [LINK07, KLOC08b]. In a dressing process with several dressing strokes, the grinding wheel surface roughness is determined by the last dressing stroke. However, the grinding wheel structure is damaged also by the previous strokes. This will result in an instationary grinding process after dressing depending on all previous dressing conditions.

6.5.4 Dressing of Superabrasive Tools

The high wear resistance of superabrasive grits provides challenges to dressing procedures. CBN grinding wheels are commonly dressed with rotating diamond tools because of the lower toughness and hardness of CBN compared to diamond [MARI07]. However, the dressing forces for CBN are higher than for conventional wheels, which needs to be considered for the dressing system design [JACK11, LINK14a]. Superabrasive wheels are dressed with much smaller depth of cut than conventional wheels [WEGE11].

Diamond grinding wheels are dressed with diamond dressing tools only in limited cases. More commonly, they vitrified bonded silicon carbide rollers are used on brake-controlled truing devices or on driven truing spindles [WEGE11, LINK14a]. The expendable and much cheaper silicon carbide wheel grinds away the diamond tool [MALK08].

Resin or metal bonded superabrasive tools sometimes require a subsequent sharpening process after the profiling process to generate sufficient grain protrusion [WEGE11]. The bonding can be set back for example with a block sharpening process [LINK14a]. Electrolytic in-process dressing (ELID) is an established method for metal bonded diamond wheels [ROWE09]. More dressing procedures using electro chemical and electro physical mechanisms exist for metal bonds [WEGE11].

6.6 Sustainability Dimensions to Grinding Wheel Micro-Design and Wear

6.6.1 Technological Dimension

Tool wear and conditioning are important factors for the tool user as they define product quality, grinding forces, maximum material removal rate and auxiliary times. Grinding tool performance impacts workpiece dimensions and surface integrity. Tool manufacturers are able to generate desired tool capabilities within a

certain range, but the tool use also decides on tool performance. Several researchers conducted detailed grinding experiments on how tool specification (structure grade, grit concentration, grit size, wheel hardness) affects grinding forces, and surface roughness and quality [LINE92, KLOM86].

6.6.2 Economic Dimension

Tool wear affects wheel life time and tool costs. However, the direct costs of different grinding wheel designs need to be compared with the total costs for process stability, auxiliary times, scrap rate, etc. (see Sect. 7.1.3 Life Cycle Costing (LCC)). Dressing is non-productive auxiliary time and the dressed wheel volume is lost for processing. The tool micro-design, i.e. abrasive layer design, defines process productivity decisively.

6.6.3 Environmental Dimension

Tool wear is waste that should be reduced to enhance material efficiency. However, as tool performance decides on product quality and scrap rate, there might be a trade-off between tool wear and scrap parts. Furthermore, trade-offs between grinding process and product performance in its use phase, defined by the surface integrity, are possible [HELU11].

Additional material output comes from wheel wear. In grinding or dressing, such high peak temperatures occur that grit and bond material melt [LINK07, ZEPP05]. Grinding tool manufacturers proved in unpublished tests that no harmful gaseous emissions derive from the grinding wheels during the machining process. Furthermore, aerosols from machinery or workpiece material are produced during grinding [RIVE07, p. 158]. Aerosols from the cooling lubricant are in particular prominent for high grinding wheel speeds.

In tool grinding of cemented carbides, cobalt leaching into the cooling lubricant can occur [REHB03]. Inhibitors and the correct choice of cooling lubricant suppress leaching [REHB03]. However, there are opposite and unproven opinions if leaching effects from metal bonds exist. The literature indicates that reactions of cooling lubricants with heavy metals or non-ferrous metals exist, but without further detailing. Inhibitors in the cooling lubricant are therefore important. Metals from the ground material can dissolve into the cooling lubricant [LIED99]. After using ester based grinding oil with vitrified bonded wheels small amounts of boron and aluminum accumulated in the oil [LIED99].

6.6.4 Social Dimension

The grinding tool user might be affected directly by grinding dust through inhalation, eye or skin contact [UNIT09b]. Respiratory problems with the grinding process emissions were already addressed in the 19th century [KNIG22]. Here, the so-called Grinder's asthma from inhaled particles was recognized and led to the development of exhaust air systems [KNIG22]. The small size of the grinding swarf or chips makes them more hazardous for the worker because they can be inhaled.

Sparks and hot chips can be dangerous, in particular when using manual grinding tools [BGI10]. Manual grinding tools are portable and therefore extra care has to be taken to remove explosive and flammable materials from the machining environment.

6.6.5 Sustainability Model for Tool Use Phase

Tool performance in the use phase is most important to the tool user, but also for the tool manufacturer and the society. The tool manufacturer is concerned with

- the **tool price**, which is a balance between the raw material and production costs and the price a tool user is willing to pay.
- **Tool wear** is an important quality factor during tool use and needs to be adjusted to the costumer satisfaction.
- **Safety** for the tool user needs to be ensured.

The tool user focuses on the technological and economic tool performance.

- **Tool wear** decides on process quality and stability as well as on process costs.
- **Dressability** is important for process setup and process stability.
- The **tool price** a tool user is willing to pay arises from the subjective tool usefulness for a certain application.
- Tool performance affects the tool user's **competitiveness**.
- The tool user needs to be sure of **safety**.
- **Hazards** from tool use and tool wear are to be avoided.

The society is interested in tool user **safety** and in **product life and performance** at a larger scale.